Icelandic
Meteorological Office

Veðurstofa Íslands

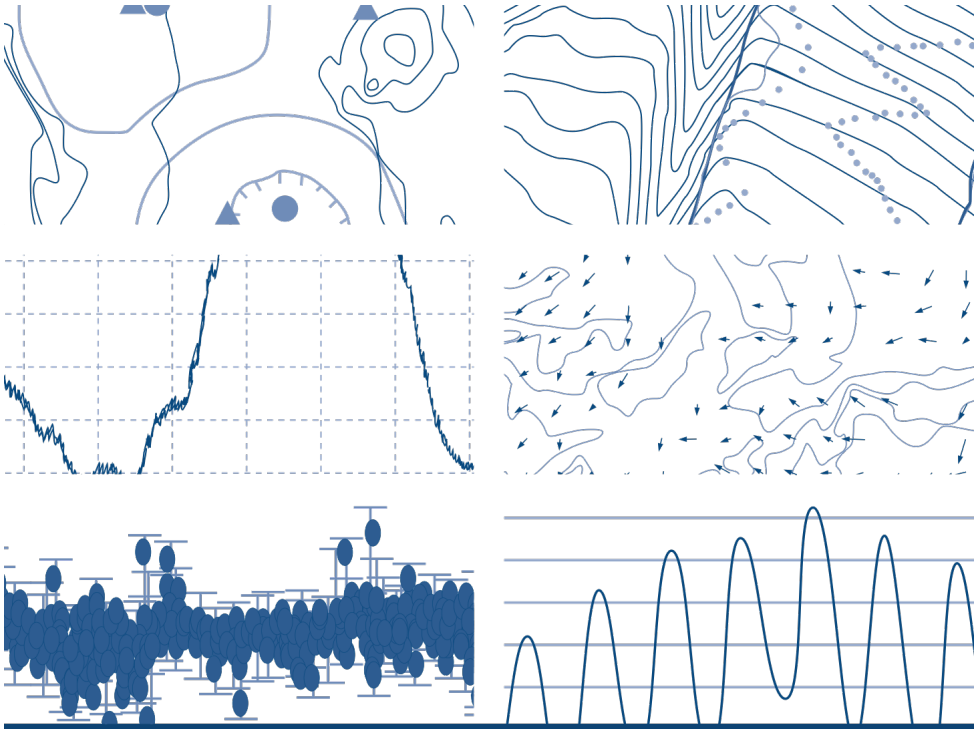

# High resolution precipitation mapping in Iceland by dynamical downscaling of ERA-40 with a linear model of orographic precipitation

Philippe Crochet

**Report**

VÍ 2012-003
[Correction p. 18]

Icelandic
Meteorological Office

Veðurstofa Íslands

# High resolution precipitation mapping in Iceland by dynamical downscaling of ERA-40 with a linear model of orographic precipitation

Philippe Crochet, Icelandic Met Office

**Report**

Veðurstofa Íslands
Bústaðavegur 7–9
150 Reykjavík

+354 522 60 00
vedur@vedur.is

VÍ 2012-003
ISSN 1670-8261

**Keypage**

Veðurstofa Íslands

| Report no.: | Date.: | ISSN: | Public ☒ Restricted ☐ |
|---|---|---|---|
| VÍ 2012-003 | April 2012 | 1670-8261 | Provision: |

| | |
|---|---|
| **Report title / including subtitle**<br>High resolution precipitation mapping in Iceland by dynamical downscaling of ERA-40 with a linear model of orographic precipitation | **No. of copies:** 10<br>**Pages:** 32+Appendix(60 pp)<br>**Managing director:**<br>Jórunn Harðardóttir |
| **Author(s):**<br>Philippe Crochet | **Project manager:**<br>Tómas Jóhannesson<br>**Project number:**<br>5811-0-0002 |
| **Project phase:** | **Case number:** |

**Report contracted for:**
CES/LOKS

**Prepared in cooperation with:**


**Summary:**
An approach based on the use of a Linear Model of orographic precipitation has recently been used to simulate a gridded daily precipitation data set with 1 km horizontal resolution for the period 1958-2006 (Crochet et al., 2007; Jóhannesson et al., 2007). The present work explores whether several refinements in the methodology and parameterization may improve the overall quality of these precipitation estimates at various temporal scales. A set of runs with different parameterizations was performed for the period 1987-2001 and the one giving the best overall results was selected and analysed in detail.



**Keywords:**
Orographic precipitation, Iceland, linear model


**Managing director's signature:**

**Project manager's signature:**

**Reviewed by:**
Tómas Jóhannesson

# Contents

# 1 Introduction

Spatially distributed precipitation estimates are needed in hydrological and glaciological modelling studies and in regional climate analyses. In Iceland, the rain gauge network is rather sparse and unevenly distributed, especially in the highlands and in complex terrain. The reason is that these regions are mainly non-inhabited, difficult to access and the presence of several large glaciers prevents the deployment of conventional precipitation gauges. Although many automatic stations have been installed in the last decade, gridding precipitation with spatial interpolation methods remains a very difficult task, especially for earlier decades, making the mapping of long-term averages, for instance, problematic.

To overcome this difficulty, an alternative approach based on a Linear Model of orographic precipitation (Smith and Barstad, 2004) was recently used to dynamically downscale the European Centre for Medium range Weather Forecasts (ECMWF) re-analysis (ERA-40) (Uppala et al., 2005) and available analysis and construct a gridded daily precipitation data set with 1 km horizontal resolution for the period 1958–2006 (Crochet et al. 2007; Jóhannesson et al. 2007). This gridded precipitation data set has since been used in hydrological modelling studies at the Icelandic Meteorological Office (IMO) (Atladóttir et al., 2011). The Linear Model combines airflow dynamics and cloud microphysics to simulate precipitation in complex terrain resulting from the terrain-forced uplift of impinging moist air. The input model parameters are background precipitation, upstream average wind speed and direction, surface temperature and humidity, moist Brunt-Väisälä frequency and hydrometeor formation and fallout times. Apart from Iceland, this model has in recent years been used in Oregon (Smith et al., 2005), California, Utah, and the Alps (Barstad and Smith, 2005), southern Andes (Smith and Evans, 2007), Norway (Schuler et al., 2008), British Columbia (Jarosh et al., 2010) and it was also used to downscale climate scenarios and study future extreme precipitation in western Norway (Carlotti and Barstad, 2010). In the work of Crochet et al. (2007) and Jóhannesson et al. (2007), the moist Brunt-Väisälä frequency and hydrometeors formation and fallout times were fixed once for all by statistical optimization, after comparison between model simulations and rain gauge and glaciological data and the same values were used for all days. The present work explores whether several refinements in the parameterization and the methodology developed at IMO may further improve the overall quality of these precipitation estimates at various temporal scales.

The proposed refinements tested in this work are as follows: First, the model is run over several sub-domains rather than for the whole of Iceland so as to better represent the spatial variability of

ambient atmospheric conditions; Second, the water vapour flux is reduced downwind along the trajectory, as suggested by Smith and Evans (2007), so as to take into account the depletion of vapour due to the production of precipitation; Third, the moist Brunt-Väisälä frequency and the hydrometeors formation and fallout times are not fixed but estimated at each time step according to ambient atmospheric conditions; Fourth, a local humidity factor is introduced to better define the areas where the model is applied when unsaturated conditions prevail, while in the previous version used at IMO, the model was applied within pre-existing wet areas defined by the large-scale precipitation fields and a fixed humidity threshold. The new model set-up was tested for a 15-year period (1987–2001) and compared to the results described by Jóhannesson et al. (2007).

In what follows, a brief model description and the proposed refinements are given in Section 2. Section 3 describes the results of the validation, considering various temporal scales and several statistical characteristics. Finally, Section 4 concludes this report.

# 2 Model description

## 2.1 The Linear theory of orographic precipitation

The Linear Model proposed by Smith and Barstad (2004) simulates precipitation over complex terrain. First, assuming that air is saturated or near saturation and flows over the terrain (no flow splitting and no stagnation), the distributed source of condensed water, $S(x,y)$, resulting from terrain-forced vertical ascent of moist air is calculated as follows:

$$S(x,y) = \frac{C_w}{H_w} \int_0^{\infty} w(x,y,z) e^{-z/H_w} dz \tag{1}$$

The vertical velocity, $w(x,y,z)$, is assumed to vary with altitude. At ground level, $w(x,y,z=0) = U \cdot \nabla h(x,y)$, where $U$ is the horizontal wind-speed vector and $\nabla h(x,y)$ the topographic gradient .

$H_w$ is the depth of the moist layer (or water vapor scale height):

$$H_w = -\frac{RT_{ref}^2}{L\gamma} \tag{2}$$

$R = 461\,J\,kg\,K^{-1}$ is the gas constant for water vapor, $L = 2.5 \cdot 10^6 J\,kg^{-1}$ is the latent heat and $T_{ref}$ is the temperature at the ground. The term $C_w = \frac{\rho_{S_{ref}} \Gamma_m}{\gamma}$ is the thermodynamics uplift sensitivity factor relating condensation rate to vertical motion, $\Gamma_m$ is the moist adiabatic lapse rate, $\rho_{S_{ref}} = \frac{e_S(T_{ref})}{RT_{ref}}$ is the saturation water vapor density and $e_S$ is the saturation vapor pressure.

The advection of condensed water by the mean wind and the resulting precipitation is described by the following equations:

$$\frac{Dq_c}{Dt} \approx U \cdot \nabla q_c = S(x,y) - \frac{q_c}{\tau_c} \tag{3}$$

$$\frac{Dq_s}{Dt} \approx U \cdot \nabla q_s = \frac{q_c}{\tau_c} - \frac{q_s}{\tau_f} \tag{4}$$

Where $q_c(x,y)$ represents the vertically integrated cloud water density, $q_s(x,y)$ represents the vertically integrated hydrometeor density, $\tau_c$ is the conversion time from cloud water into hydrometeors, $\tau_f$ is the hydrometeor fallout time and $q_s/\tau_f$ represents the precipitation rate.

The solution of Eqs. (3) and (4) is obtained by taking the Fourier transforms of Eqs. (1), (3) and (4). The dynamics of the forced ascent, $w(x,y,z)$, is described using results from mountain wave theory, which in Fourier space leads to $\widehat{w}(k,l,z) = \widehat{w}(k,l,0)e^{imz}$, with $\widehat{w}(k,l,0) = i\sigma\widehat{h}(k,l)$. The term $\sigma = U_x k + U_y l$ is the intrinsic frequency which defines the wind vector in Fourier space, k and l the horizontal wave numbers, $m = [\frac{N_m^2-\sigma^2}{\sigma^2}(k^2+l^2)]^{1/2}$ the vertical wave number and $N_m$ the moist Brunt-Väisälä frequency. After some algebra, the double Fourier transform of the precipitation field $\widehat{P}(k,l)$ is given by the following transfer function:

$$\widehat{P}(k,l) = \frac{C_w i\sigma\hat{h}(k,l)}{(1-imH_w)(1+i\sigma\tau_c)(1+i\sigma\tau_f)}, \tag{5}$$

where the double Fourier transform of the terrain $\widehat{h}(k,l)$ is given by

$$\widehat{h}(k,l) = (2\pi)^{-2}\int\int h(x,y)e^{-i(kx+ly)}dx\,dy. \tag{6}$$

Eq. (5) states that precipitation is controlled by several partly counteracting processes, namely airflow dynamics, cloud time scales and the advection of condensed water and hydrometeors.

The amount of water vapor that can be condensed (the source term $S(x,y)$) depends on the moist layer depth and the ability of the forced vertical ascent to penetrate through this moist layer, which is controlled by airflow dynamics. The condensation is reduced if the vertical uplift does not penetrate through the moist layer. Also, an increase of stability ($N_m$) will cause the available water vapor to increase ($C_w$ and $H_w$) but will reduce the depth of the lifting (increasing $m$).

If $\tau_c$ is short, then condensed water will be formed quickly on the windward side and start to precipitate before being advected downstream to the lee-side of the mountain where it evaporates. If $\tau_f$ is short, then precipitation will mainly fall on the windward side of the mountain while if it is long, spill-over will take place and precipitation will also fall on the lee-side. This also means that for given $\tau_c$ and $\tau_f$ values, the resulting precipitation pattern will depend on the width of the mountain and the wind-speed. High wind speeds may advect air parcels over the lee-side before water vapor has time to condense and fall. Large values of $\tau_c$ and $\tau_f$ will shift the condensation and precipitation downstream. The residence time of an air-parcel on the windward side of a large mountain will be longer than on a smaller one, increasing the amount of water that can be condensed and precipitation that can be formed.

A detailed description of changes in spatial precipitation patterns and location of maximum precipitation in response to changing atmospheric conditions, mountain geometry and horizontal topographic scales can be found in Smith and Barstad (2004) and Barstad and Smith (2005).

The precipitation field is finally retrieved after taking the inverse Fourier transform of (5) and truncating negative values of the total precipitation to simulate downslope evaporation:

$$P(x,y) = Max[(\int_{-\infty}^{\infty}\int_{-\infty}^{\infty}\widehat{h}(k,l)e^{i(kx+ly)}dk\,dl + P_{\infty}), 0] \tag{7}$$

The term $P_{\infty}$ represents the pre-existing background precipitation resulting from synoptic-scale uplift.

## 2.2 Model parameterization and set-up

The model was run with input meteorological data from the ECMWF re-analysis (ERA-40), with a time step of 6 hours. The same strategy as defined in Jóhannesson et al. (2007) was used. The Linear Model is first applied using the ERA-40 orography to estimate the orographic precipitation that might already be present in the background precipitation and removed, in order not to doublecount it. Background precipitation lower than 0.15mm/6h is set to 0. Then, the Linear Model is applied using the true orography and the corrected background precipitation.

**Moist Brunt-Väisälä frequency**

The moist Brunt-Väisälä frequency ($N_m$) was estimated after Durran and Klemp (1982) as

$$N_m^2 = \frac{g}{T}(\frac{dT}{dz} + \Gamma_m)(1 + \frac{Lq_s}{RT}) - \frac{g}{1+q_w}\frac{dq_w}{dz} \tag{8}$$

where $\Gamma_m$ is the moist adiabatic lapse rate

$$\Gamma_m = \Gamma_d(1+q_w)(1+\frac{Lq_s}{RT}) \times \{1 + \frac{c_{pv}q_s + c_w q_L}{c_p} + \frac{\varepsilon L^2 q_s}{c_p RT^2}(1+\frac{q_s}{\varepsilon})\}^{-1} \tag{9}$$

and $\Gamma_d$ is the dry adiabatic lapse rate

$$\Gamma_d = \frac{g}{c_p}. \tag{10}$$

$g$ is the gravitational acceleration, $c_p$, $c_{pv}$ and $c_w$ are the heat capacities of dry air, water vapor and liquid water respectively, $\varepsilon = 0.622$ is the ratio of the gas constants for dry air and water vapor, $q_w = q_s + q_L$ is the total water mixing ratio, $q_s$ is the saturation mixing ratio and $q_L$ the cloud liquid water mixing ratio.

**Hydrometeors formation and fallout times**

The hydrometeors formation time, $\tau_c$, and fallout time, $\tau_f$, were parameterized according to Kunz and Kottmeier (2006) and Sinclair (1994), respectively as

$$\tau_c = t_{ice}(0.5 + \frac{1}{\pi}\arctan(\frac{z-(z_m+\Delta z)}{500})), \tag{11}$$

where $t_{ice}$ is the formation time of ice particles aloft, $z_m$ is the height of the melting layer and $\Delta z$ is the distance below the freezing level at which ice particules are assumed to melt completely. This formulation was derived from Sinclair (1994)

$$\tau_c = 1000(0.5 + \frac{1}{\pi}\arctan(\frac{p_m - p}{50})), \tag{12}$$

where $p$ is the pressure level and $p_m$ is 50 hPa below the freezing level.

At a given level, raindrops were assumed to fall with a velocity $v_f = \frac{\alpha q}{q_{surf}}$m/s, where $q$ is the mixing ratio at the given level and $q_{surf}$ at the surface and $\alpha = 6$, according to Sinclair (1994). Above the freezing level, snow is assumed to fall with a speed of $\frac{q}{q_{fz}}$m/s where $q_{fz}$ is the mixing ratio at the freezing level, which means that at the freezing level, snow falls at 1m/s. The fall speed was calculated for each model layer and then averaged and the fallout time was estimated through the moist layer.

**Humidity factor**

In both Crochet et al. (2007) and Jóhannesson et al. (2007), the use of the Linear Model was restricted within pre-existing wet areas defined by the background precipitation fields and a constant humidity threshold so as to guaranty that near saturated conditions were met. In this version, a local humidity factor was introduced as suggested by Sinclair (1994) so as to better define the limits of application of the model and reduce precipitation when unsaturated conditions prevail. In Sinclair (1994), this humidity factor is defined as

$$\lambda(x,y) = \begin{cases} (\frac{RH_{x,y,l} - RH_{min}}{\beta})^{\delta} & \text{if } RH_{x,y,l} > RH_{min}, \\ 0 & \text{otherwise} \end{cases} \tag{13}$$

where $RH_{x,y,l}$ is the low-level relative humidity, taken at 850-hPa, $RH_{min}$ is the lower RH threshold below which no orographic precipitation is formed, $\beta$ and $\delta$ are adjustable parameters taken as $RH_{min} = 0.8$, $\beta = 0.2$ and $\delta = 0.25$. A similar function was used in Kunz and Kottmeier (2006) with $RH_{x,y,l}$ taken at 1.5km and identical values for $RH_{min}$, $\beta$ and $\delta$ which were confirmed by a sensitivity analysis. In this work, another formulation was also tested:

$$\lambda(x,y) = \begin{cases} 1 - \exp(-(\frac{RH_{x,y,l} - RH_{min}}{\phi})^{\Psi}) & \text{if } RH_{x,y,l} > RH_{min} \\ 0 & \text{otherwise} \end{cases} \tag{14}$$

Precipitation is then corrected as follows

$$P_{corr}(x,y) = P(x,y)\lambda(x,y) \tag{15}$$

**Reduced water vapor flux**

In the original formulation (Smith and Barstad, 2004), the Linear Model expresses precipitation as proportional to the upstream water vapor flux. In the case of a domain with a succession of

mountain ridges, the water vapor flux is in fact depleted downwind once the airflow has passed over several hills and orographic precipitation has formed. In order to deal with this, Smith and Evans (2007) made the assumption that precipitation is proportional to the local water vapor flux and proposed to scale the precipitation down with the local fraction of water vapor remaining, as follows

$$P_{reduced}(x,y) = P(x,y)\Theta(x,y), \tag{16}$$

where $P(x,y)$ is computed with Eq. (7) and $\Theta(x,y)$ is the fraction of vapor remaining defined as

$$\Theta(x,y) = 1 - \int_{-\infty}^{x,y} P_{reduced}(x',y')ds/F_0. \tag{17}$$

Where $F_0 = \rho q_w U H_w$ is the incoming upstream horizontal water vapor flux and $ds = (U_x dx' + U_y dy')/|U|$. After some manipulations this leads to:

$$\Theta(x,y) = e^{-DR_{ref}(x,y)}, \tag{18}$$

where

$$DR_{ref}(x,y) = \int_{-\infty}^{x,y} P(x',y')ds/F_0. \tag{19}$$

In our case, $P(x,y)$ is replaced by $P_{corr}(x,y)$ in (16) and (19) and the final precipitation estimate is given as

$$P_{reduced}(x,y) = P_{corr}(x,y)\Theta(x,y). \tag{20}$$

**Model set-up**

The methodology described above was applied using several strategies, which are not all described in detail here. The different tests include varying the values for the parameters $t_{ice}$, $\alpha$, $RH_{min}$, $\beta$, $\delta$, $\phi$, $\psi$, varying the horizontal and vertical domains of calculation for the mean $U_x$, $U_y$, $N_m$, $\tau_c$ and $\tau_f$, imposing lower and upper limits for the hydrometeor fallout velocity, and testing several strategies for calculating the reduction of the water vapor flux.

**Multi-domain runs**

For each model set-up, the model was run three times per time step over the entire domain so as to better represent the spatial variability of ambient atmospheric conditions, especially the mean wind whose direction may vary within the domain and will have a strong impact on the spatial pattern of precipitation. In practise, the input meteorological parameters (except the background precipitation) where calculated for three different sub-domains and the Linear Model applied each time to the entire domain but the resulting precipitation corresponding to each sub-domain only was selected. The final precipitation map was obtained by merging the precipitation from

each sub-domain. These domains roughly correspond to homogeneous climatic zones and were defined according to the topography so as to have a natural border and avoid sharp transitions between sub-domains (see Figure 1).

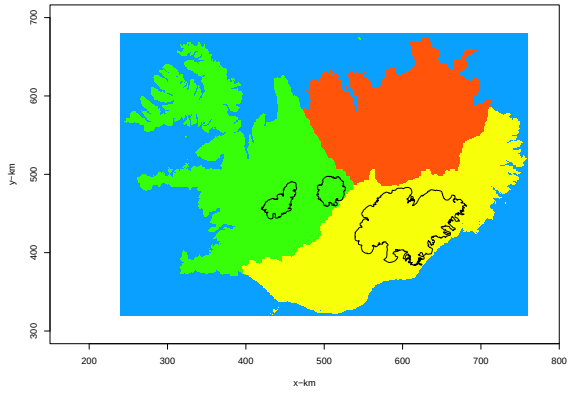


*Figure 1. The domains for the multi-runs.*

# 3 Validation

## 3.1 Objective functions

Experience usually shows that a single model parameterization may not yield the best simulations for all features of the observed precipitation field or its statistical properties. The reason being that errors affect both observed precipitation and input model parameters (or their mean estimates), and that the model is an imperfect representation of the physical processes taking place in reality. Moreover, users may be interested to simulate specific features more accurately than others. For all these reasons, the validation was conducted with a multi-objective goal in mind and several statistical criteria were used in order to measure different properties of the simulated precipitation fields:

- The mean error (ME):

$$ME = E[P^* - P] \tag{21}$$

- The root mean square error (RMSE):

$$RMSE = \sqrt{E[(P^* - P)^2]} \tag{22}$$

- The Nash & Sutcliffe efficiency criterion ($R^2$):

$$R^2 = 1 - \frac{\sum_i (P_i^* - P_i)^2}{\sum_i (P_i - E[P])^2} \qquad where - \infty \leq R^2 \leq 1 \tag{23}$$

In Eqs. (21)–(23), $P$ and $P^*$ represent the observed and simulated precipitation (Eq. 20), respectively, and $i$ the time index.

These criteria were calculated for different response variables such as annual precipitation, winter precipitation, monthly precipitation and 3-day precipitation. As daily simulations were accumulated from 12UTC to 12UTC and precipitation is measured from 09UTC to 09UTC, the 3-day precipitation was used instead of daily precipitation so as to analyse precipitation for a short integration time and minimize the discrepancy due to these timing difference. Nevertheless, several statistical characteristics of daily precipitation were considered, such as the mean, several quantiles and the Probability of Precipitation (PoP) above several thresholds, and in this case the timing difference between simulations and observations becomes irrelevant, assuming that precipitation is not affected by diurnal variations. The precipitation of reference was derived from precipitation observations at the raingauge stations after wind-loss correction, as described in Crochet et al. (2007). In addition, winter precipitation was derived from mass-balance measurements made on three glaciers: Vatnajökull, Hofsjökull and Langjökull. The raingauge data were further split into three groups, namely stations located in i) open (or relatively gentle) terrain, ii) windward (or enhancement) terrain and iii) lee-side (or rain-shadow) terrain, respectively, according to the dominating wind-direction, as in Crochet et al. (2007) and in Jóhannesson et al. (2007). In practice, as wind direction is variable, a given station may alternatively be located on the windward side or the lee-side. The verification network is presented in Figure 2.

In order to select the best overall model set-up, each run was ranked and given a score between 0 (worst) and 1 (best) according to each statistical criteria. The best overall model set-up was derived by a weighted sum of these scores (derived from NASH and ME) in an attempt to reflect the trade-offs among the set of objectives and the different response variables. Finally, the results obtained with the selected model set-up were thoroughly examined, annual precipitation maps were inspected for consistency and all these results compared with the reference precipitation described in Jóhannesson et al. (2007).

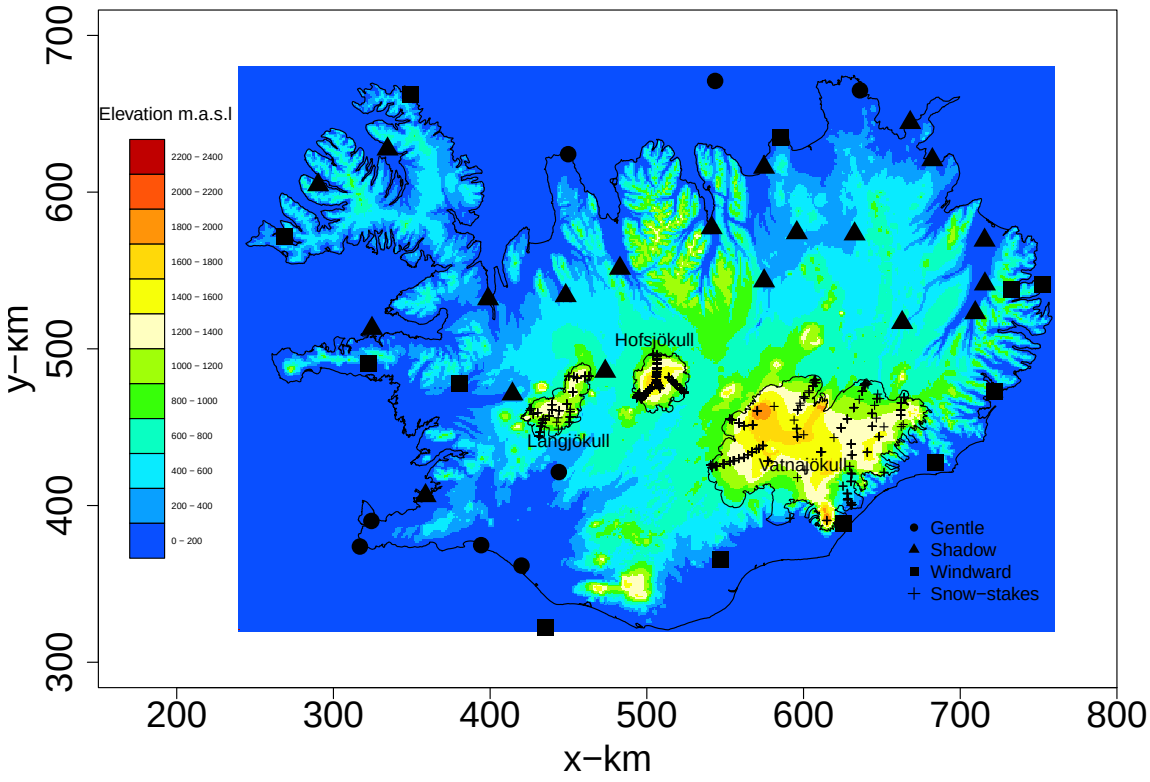


*Figure 2. Topography and location of raingauge network and snow-stakes used in the validation.*

## 3.2 Results

The selected model set-up giving the best overall score according to the methodology defined in the previous section corresponds to the following methodology:

- Humidity factor

$$\lambda(x,y) = \begin{cases} 1-\exp(-(\frac{RH_{x,y,850-hPa}-0.8}{0.125})^4) & \text{if } RH_{x,y,850-hPa} > 0.8 \\ 0 & \text{otherwise} \end{cases} \quad (24)$$

  A comparison between this humidity factor and the one given by Sinclair (1994), Eq. (13) is given in Figure 3.

- Cloud water conversion time

$$\tau_c = 1200(0.5 + \frac{1}{\pi}\arctan(\frac{z-(z_m+200)}{500})) \quad (25)$$

- Hydrometeor fall velocity

$$v_f = \begin{cases} \frac{5q}{q_{surf}} & \text{if } 0.1 \leq v_f \leq 5\text{m/s} \\ 0.1 & \text{if } v_f < 0.1\text{m/s} \\ 5 & \text{if } v_f > 5\text{m/s} \end{cases} \quad (26)$$

- Water vapor flux correction
  The water vapor flux correction is calculated after taking into account the fact that vapor is also removed from the airstream by the background precipitation:

$$F_\infty = \int_{-\infty}^{x,y} P_\infty(x',y')ds \quad (27)$$

  The drying ratio is given by:

$$DR_{ref}(x,y) = \int_{-\infty}^{x,y} P(x',y')ds/(F_0 - F_\infty) \quad (28)$$

  And finally the correction coefficient used to scale the precipitation down is obtained as follows:

$$\Theta(x,y) = e^{-DR_{ref}(x,y)} \quad (29)$$

- Other features

  The column-averaged wind was calculated at each grid point within a vertical column extending approximately from 250 m a.s.l to 1000 m a.s.l, i.e. from half to twice the average altitude of Iceland and then further averaged over each sub-domain (and not upstream). The cloud water conversion time, $\tau_c$ and fallout time $\tau_f$ were calculated over each sub-domain considering a vertical column corresponding to the moist layer depth $H_w$ starting at the mean altitude of Iceland, 505 m a.s.l. The moist layer depth was estimated upstream of each sub-domain given the low-level wind direction calculated over each sub-domain.

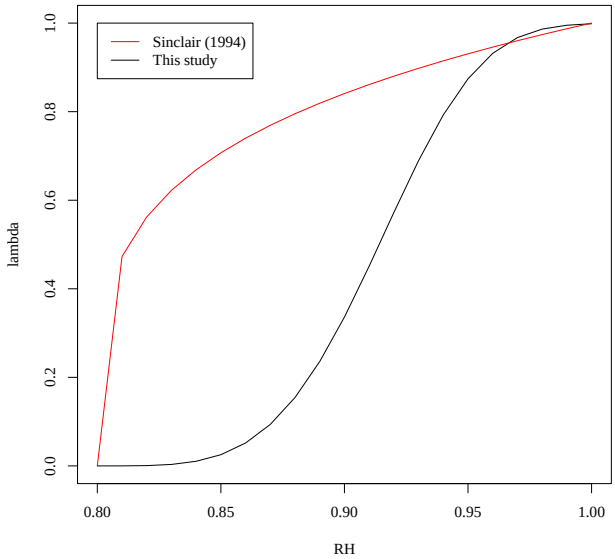


*Figure 3. Humidity factor.*

Table 1 presents all the statistical scores for both the selected new model version and the reference model version (Jóhannesson et al., 2007). Figures 4 to 6 present maps of the statistics of annual precipitation for the period 1987–2001 and Figure 7 presents the difference between maximum and minimum annual precipitation over the 15-year period. Figure 8 presents scatter plots between observed and simulated annual precipitation, Figure 9 presents scatter plots between observed and simulated monthly precipitation, Figure 10 presents scatter plots between observed and simulated 3-day precipitation and Figures 11 to 13 present scatter plots between observed and simulated daily precipitation statistics calculated at each station and for each year. Additional results can be found in the Appendix.

*Table 1. Error statistics. Best model version for ME (blue) and for Nash (R2) (red).*

| Variable/Statistics | ME ref | ME new | R2 ref | R2 new |
|---|---|---|---|---|
| Annual precipitation (open terrain) | -116.4 | -134.8 | 0.269 | 0.52 |
| Annual precipitation (rain-shadow terrain) | -89.6 | -81.4 | 0.61 | 0.55 |
| Annual precipitation (windward terrain) | -210.5 | -173 | 0.64 | 0.78 |
| Monthly precipitation (open terrain) | -10.3 | -10.9 | 0.54 | 0.6 |
| Monthly precipitation (rain-shadow terrain) | -5.01 | -2.7 | 0.56 | 0.5 |
| Monthly precipitation (windward terrain) | -14.1 | -9.6 | 0.587 | 0.69 |
| 3-day precipitation (open terrain) | -1.22 | -1.31 | 0.53 | 0.54 |
| 3-day precipitation (rain-shadow terrain) | -0.7 | -0.60 | 0.48 | 0.46 |
| 3-day precipitation (windward terrain) | -1.58 | -1.34 | 0.50 | 0.55 |
| Winter precipitation (Vatnajökull) | 20 | 45.4 | 0.32 | -0.26 |
| Winter precipitation (Hofsjökull) | -15.4 | 268.2 | 0.56 | 0.22 |
| Winter precipitation (Langjökull) | -280.8 | -54.4 | -0.76 | -1.42 |
| Mean daily precipitation (open terrain) | -0.63 | -1.09 | 0.28 | 0.02 |
| Mean daily precipitation (rain-shadow terrain) | -0.09 | -0.44 | 0.47 | 0.17 |
| Mean daily precipitation (windward terrain) | -0.89 | -1.43 | 0.63 | 0.64 |
| 25% daily precipitation quantile (open terrain) | 0.71 | 0.26 | -6.19 | -0.44 |
| 25% daily precipitation quantile (rain-shadow terrain) | 0.48 | 0.23 | -6.58 | -1.49 |
| 25% daily precipitation quantile (windward terrain) | 1.01 | 0.2 | -5.81 | 0.25 |
| 50% daily precipitation quantile (open terrain) | 0.75 | 0.1 | 0.26 | 0.74 |
| 50% daily precipitation quantile (rain-shadow terrain) | 0.79 | 0.37 | -6.2 | -1.5 |
| 50% daily precipitation quantile (windward terrain) | 1.54 | 0.03 | 0.1 | 0.79 |
| 95% daily precipitation quantile (open terrain) | -5.85 | -6.08 | -2.11 | -2.01 |
| 95% daily precipitation quantile (rain-shadow terrain) | -2.98 | -3.6 | 0.19 | -0.12 |
| 95% daily precipitation quantile (windward terrain) | -10.6 | -8.3 | -0.24 | 0.31 |

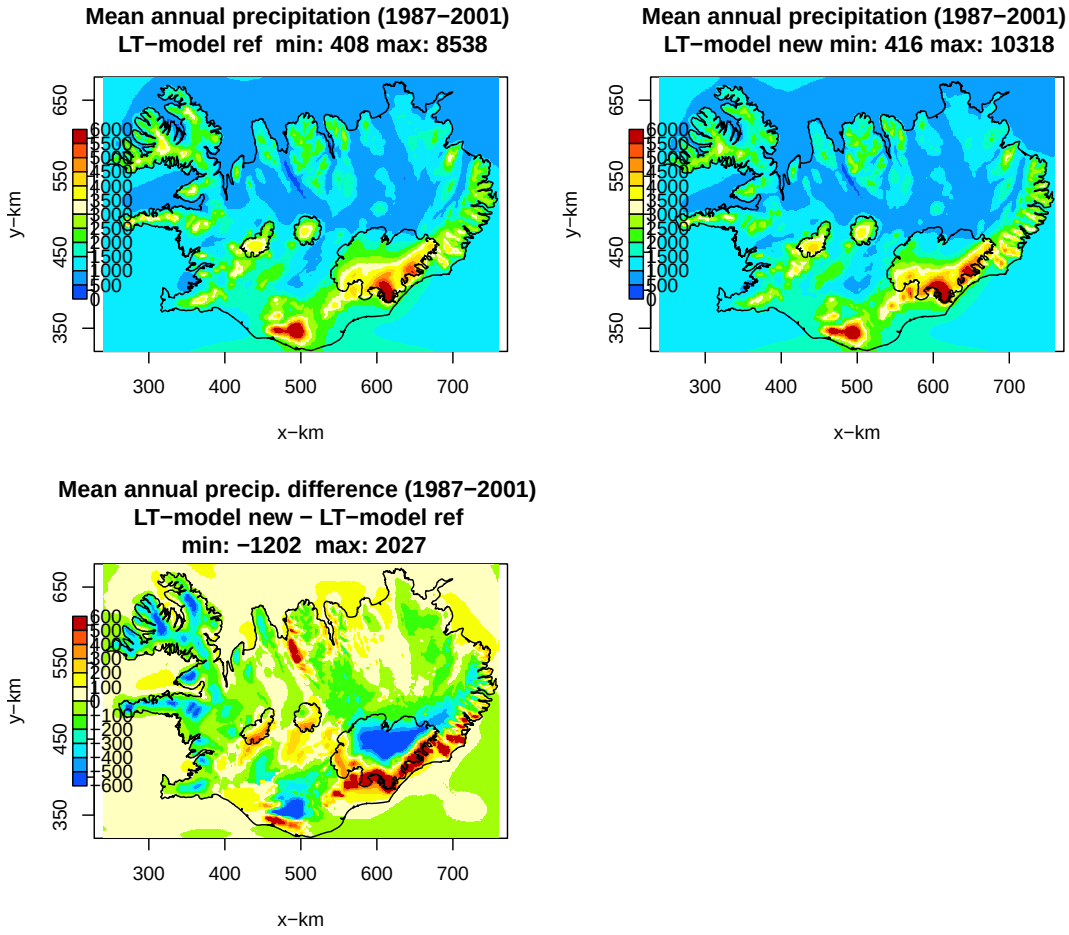


*Figure 4. Mean annual precipitation map (1987–2001) simulated with the reference model version (top-left) and the new model version (top-right), and the difference between the new and reference maps (bottom).*

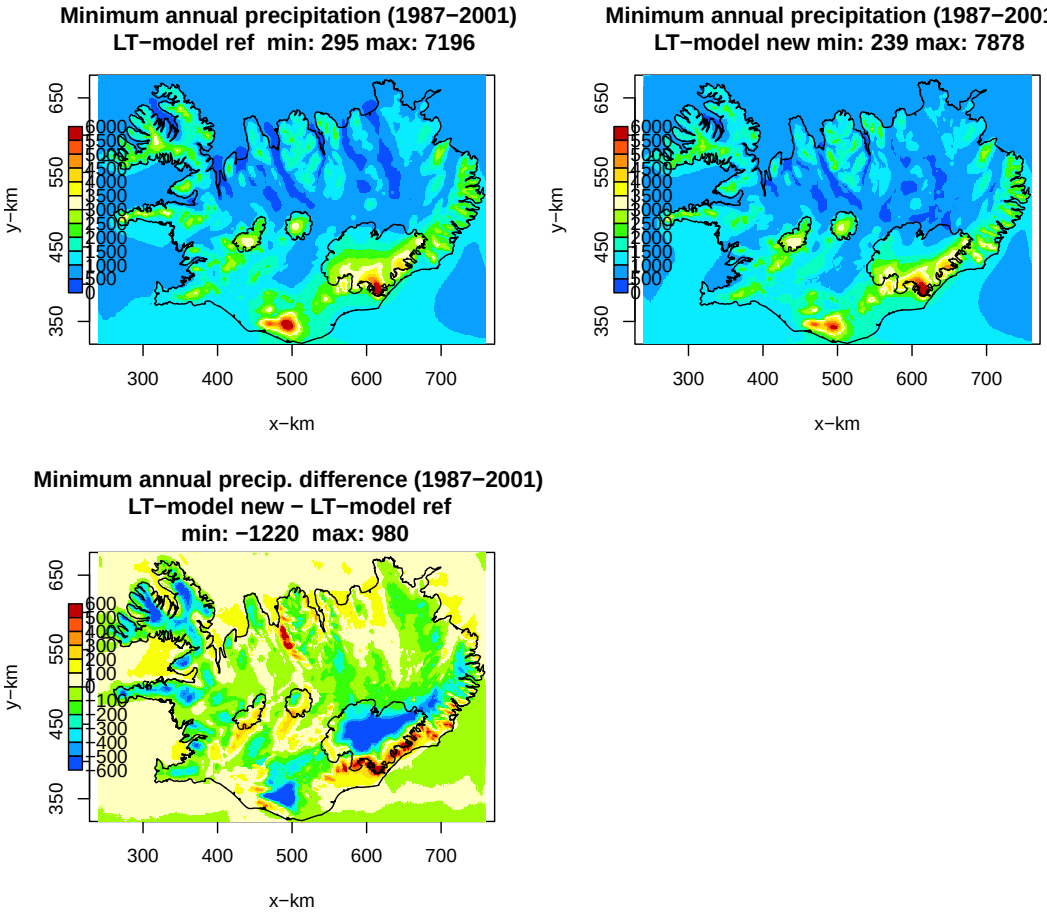


*Figure 5. Minimum annual precipitation map (1987–2001) simulated with the reference model version (top-left) and the new model version (top-right), and the difference between the new and reference maps (bottom).*

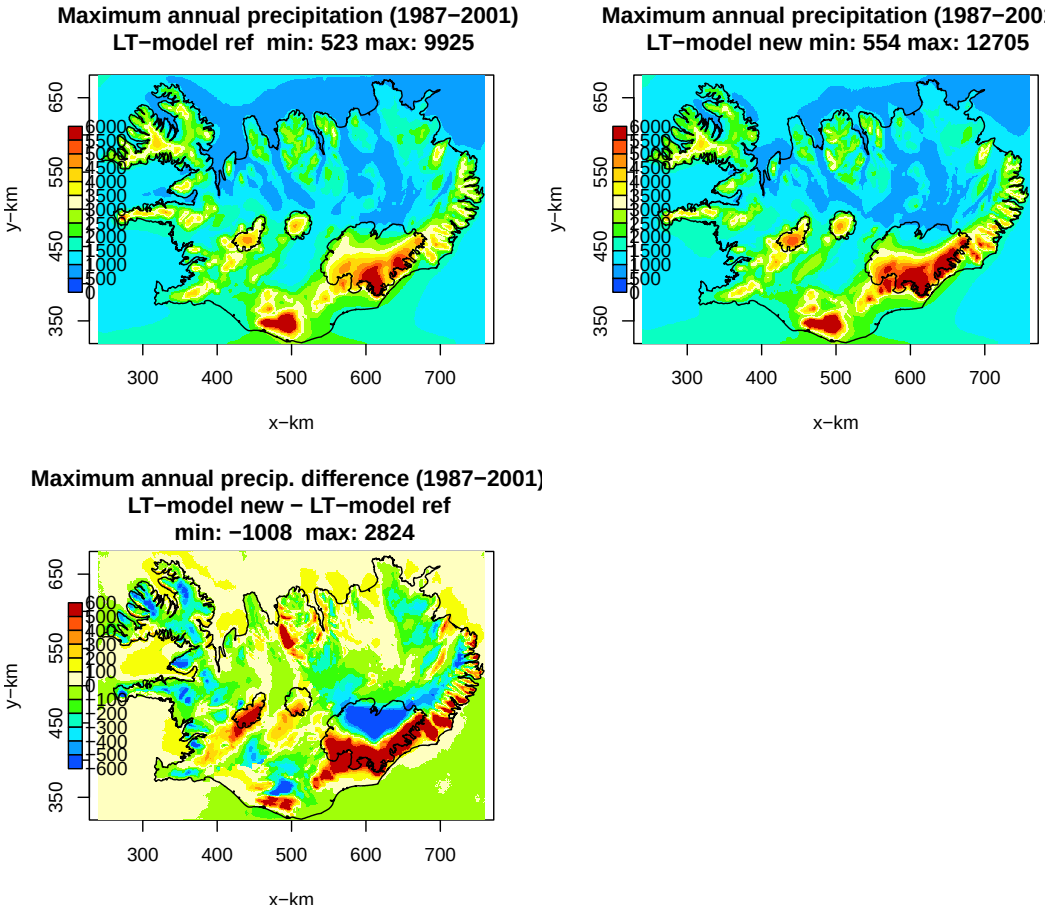


*Figure 6. Maximum annual precipitation map (1987–2001) simulated with the reference model version (top-left) and the new model version (top-right), and the difference between the new and reference maps (bottom).*

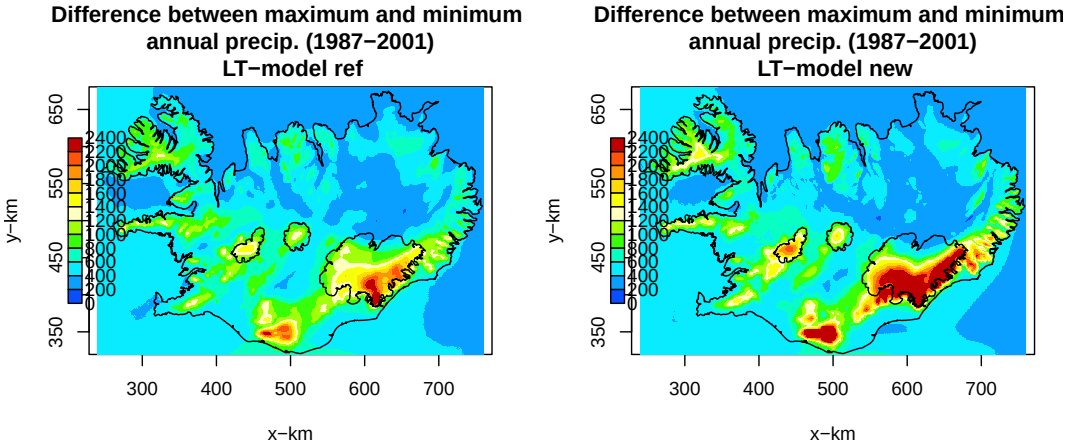


*Figure 7. Difference between maximum and minimum annual precipitation (1987–2001) simulated with the reference model version (left) and the new model version (right).*

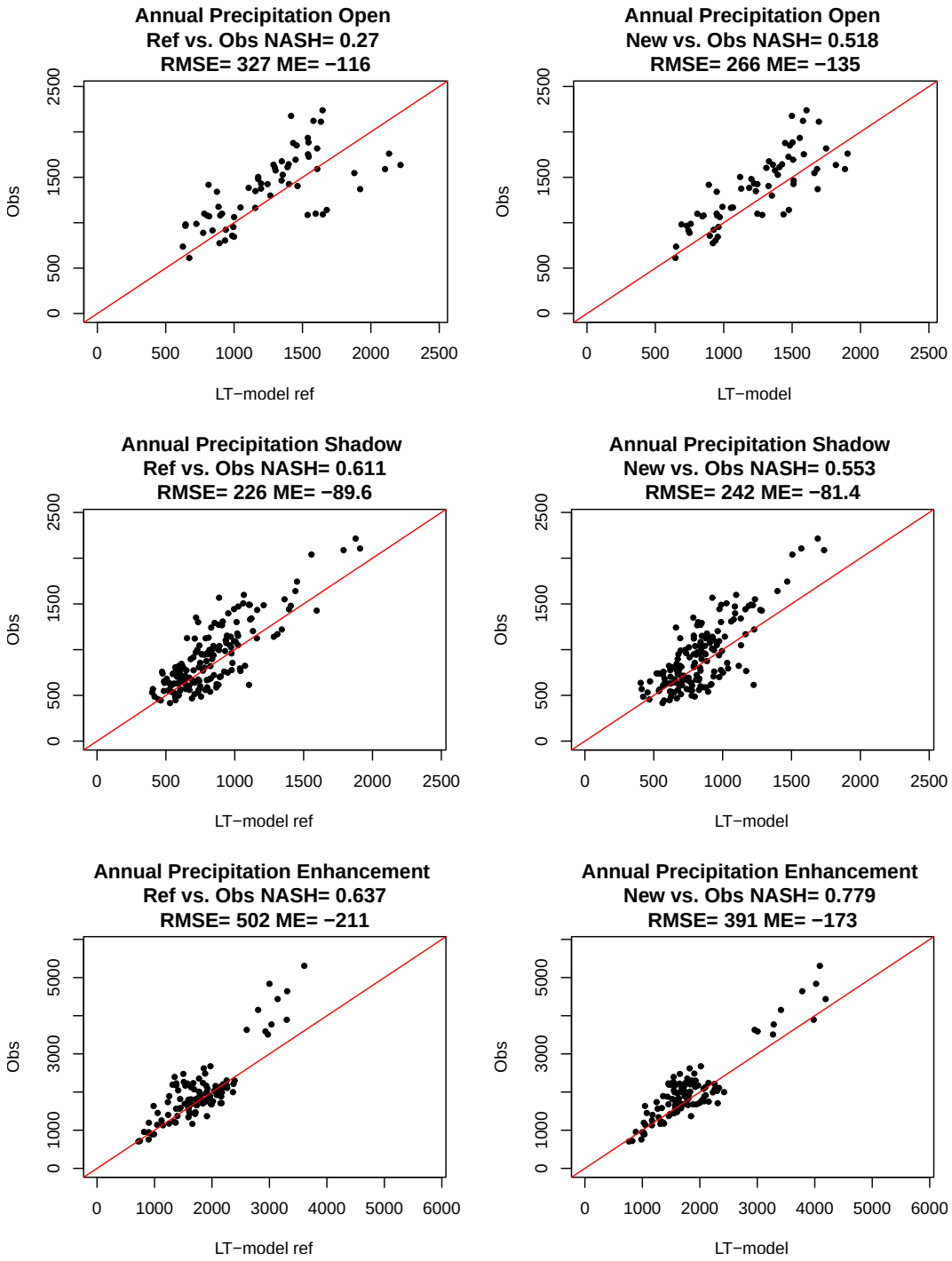


*Figure 8. Annual precipitation at stations located in open terrain (top), rain-shadow (middle) and windward terrain (bottom), simulated with the reference model version (left) and the new model version (right).*

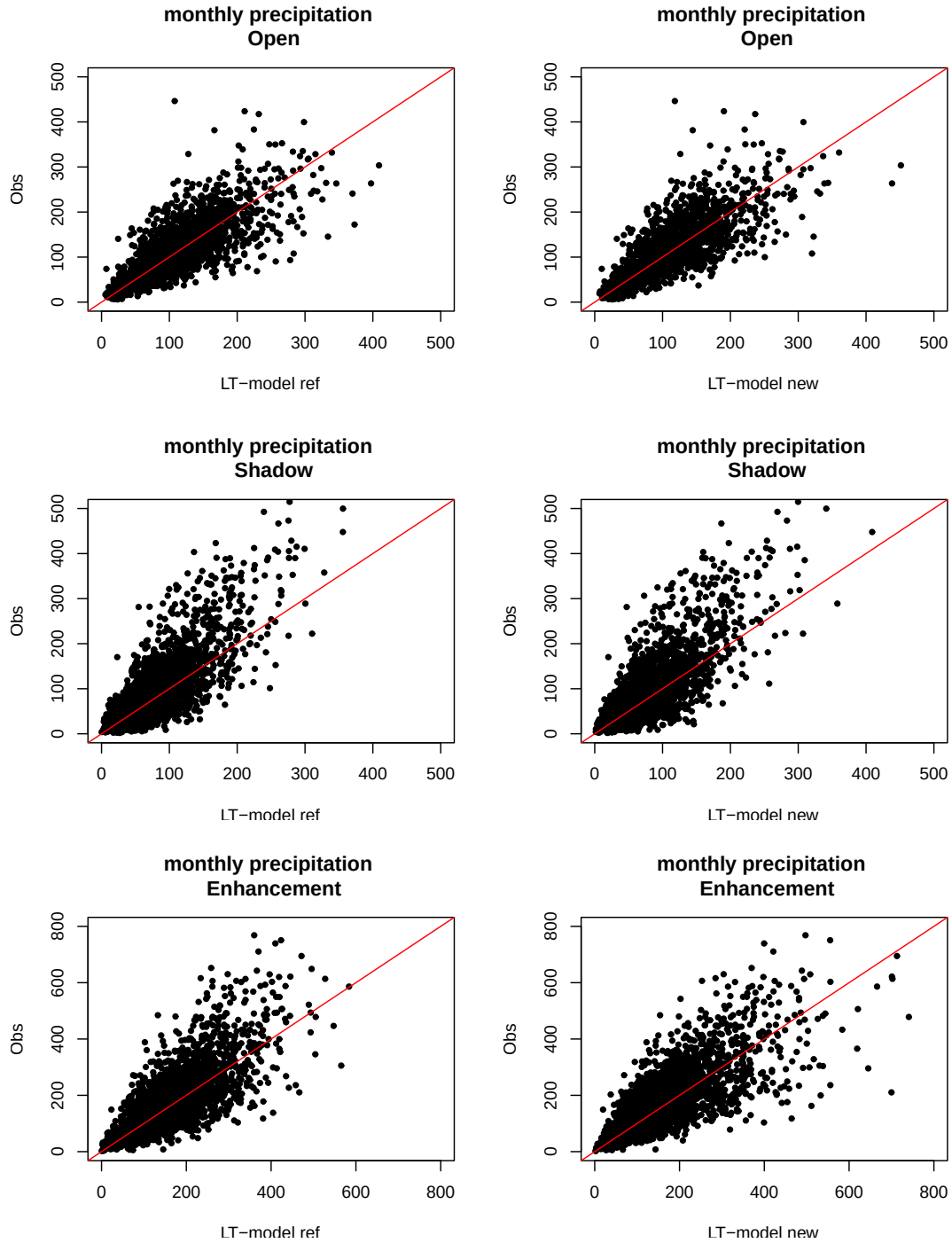


*Figure 9. Monthly precipitation at stations located in open terrain (top), rain-shadow (middle) and windward terrain (bottom), simulated with the reference model version (left) and the new model version (right).*

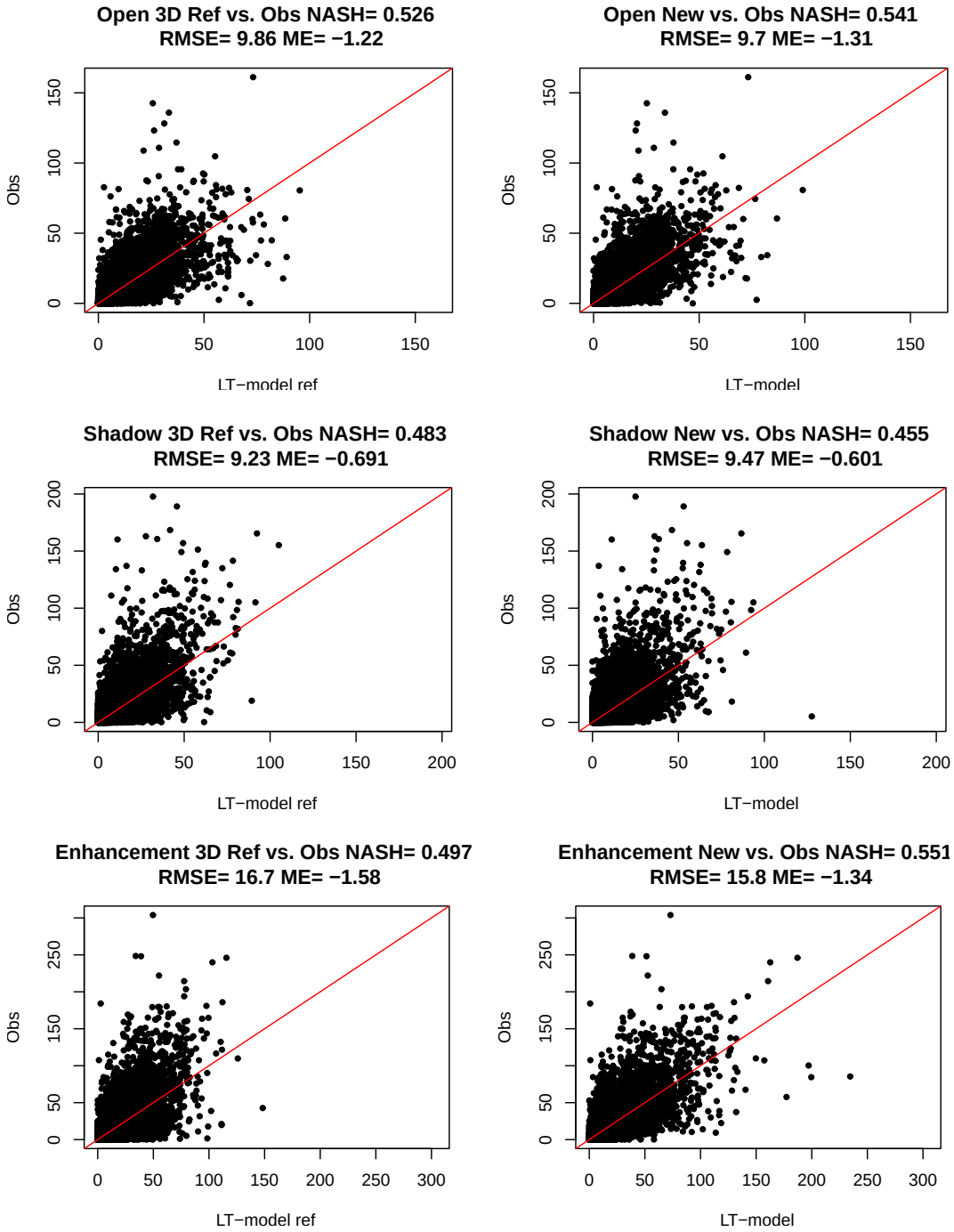


*Figure 10. 3-day precipitation at stations located in open terrain (top), rain-shadow (middle) and windward terrain (bottom), simulated with the reference model version (left) and the new model version (right).*

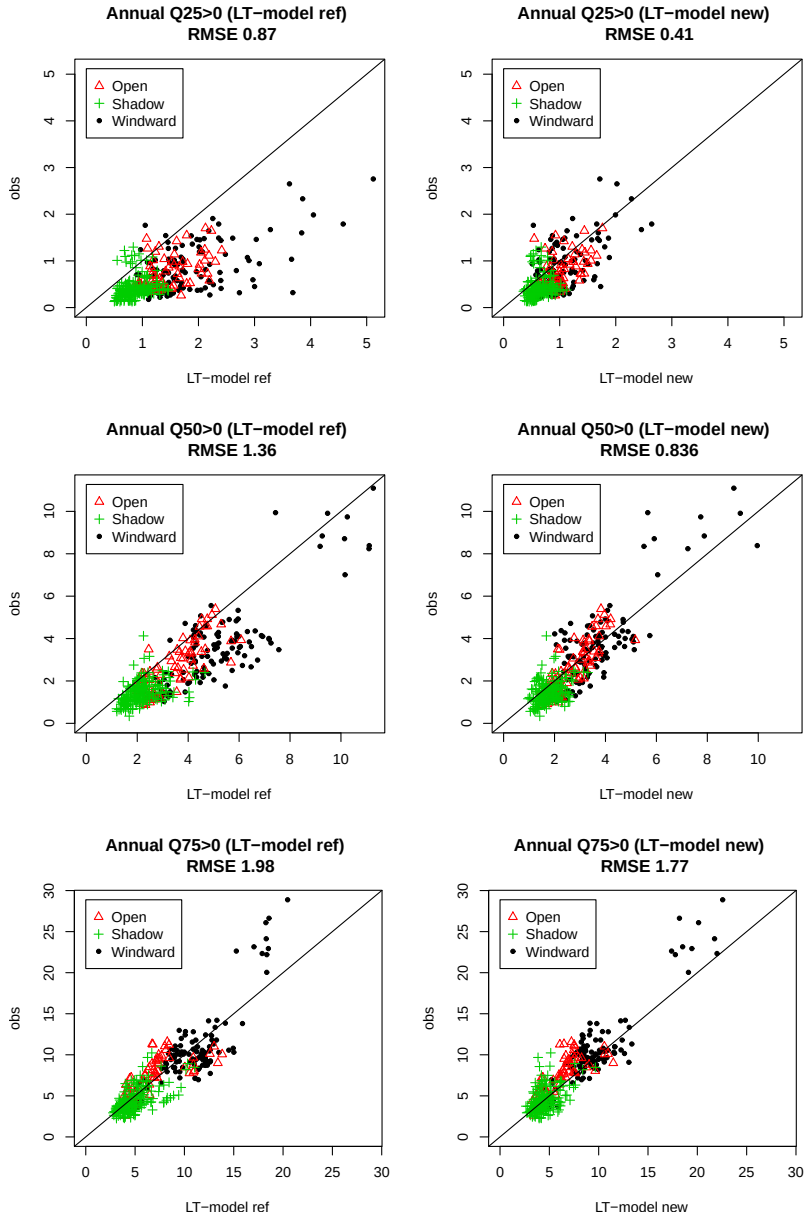


*Figure 11. Annual statistics for strictly positive daily precipitation (1991–2000): 25% quantile (top), 50% quantile (middle) and 75% quantile (bottom) at each station, simulated with the reference model version (left) and the new model version (right).*

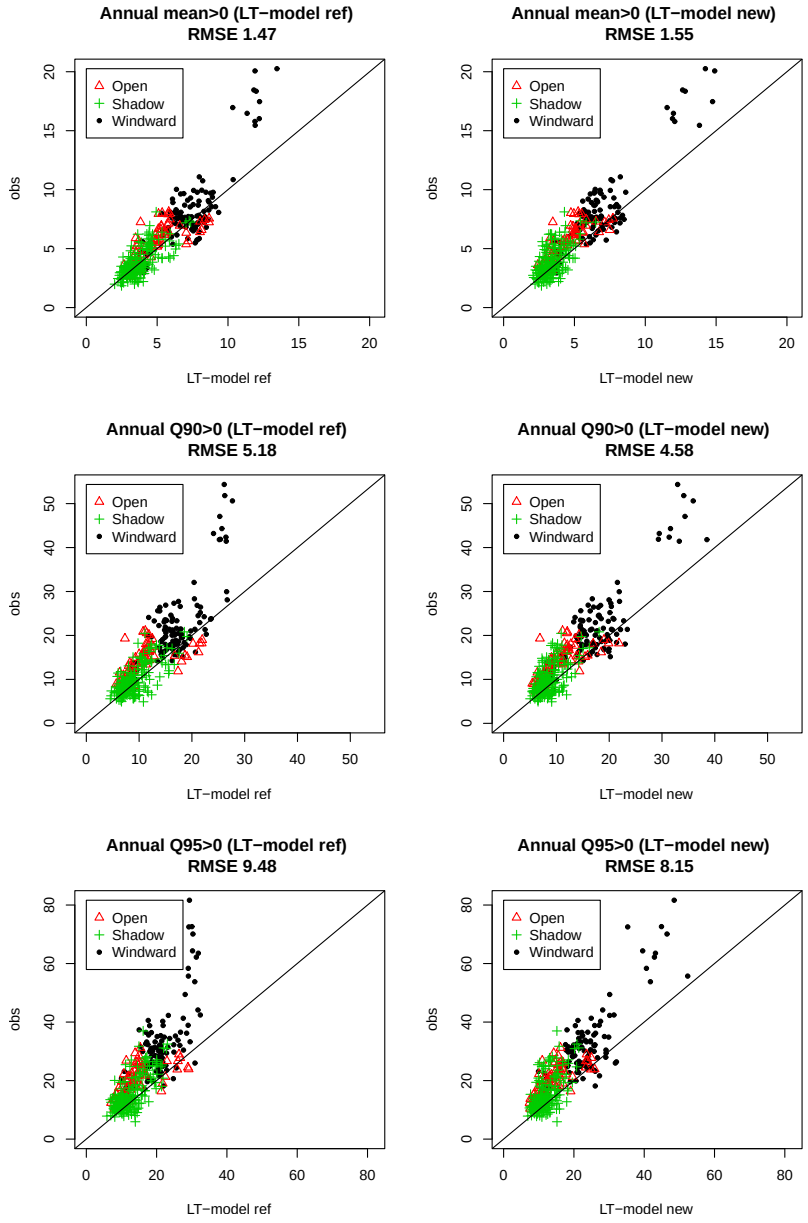


*Figure 12. Annual statistics for strictly positive daily precipitation (1991–2000): mean (top), 90% quantile (middle) and 95% quantile (bottom) at each station, simulated with the reference model version (left) and the new model version (right).*

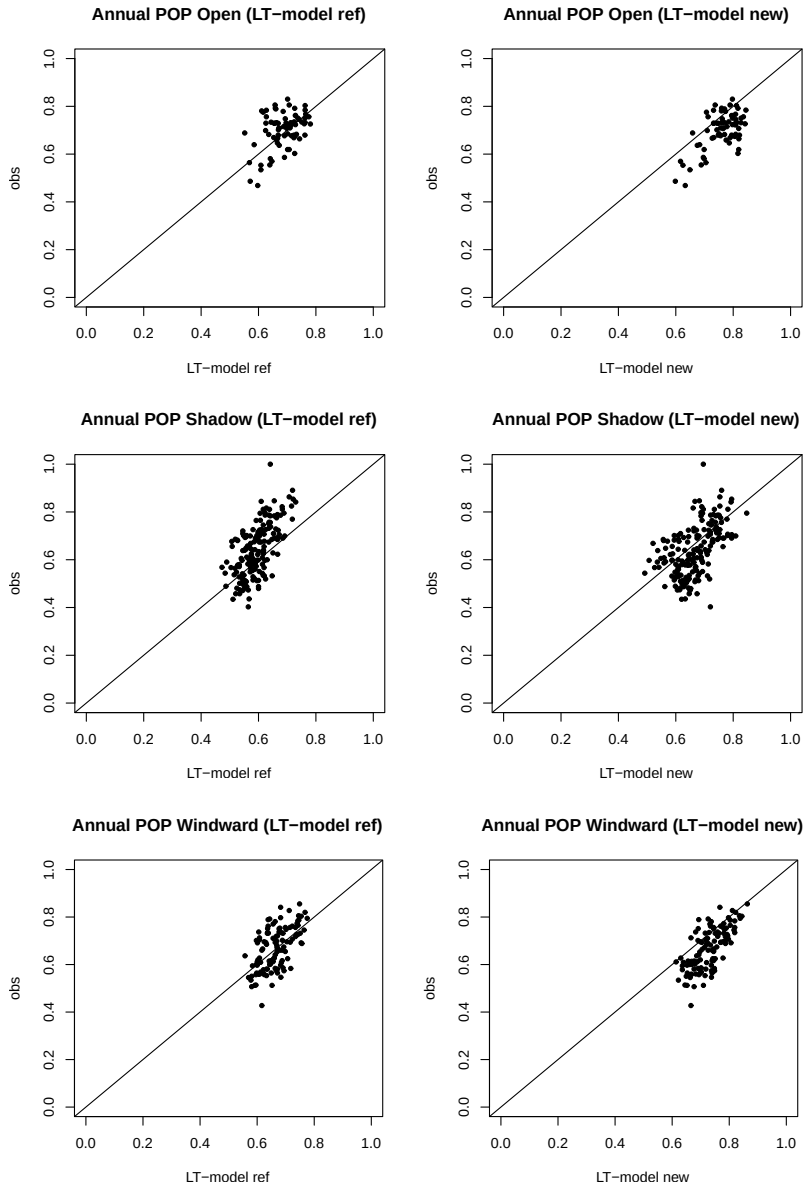


*Figure 13. Annual Probability of Precipitation above 0.1mm/day (1991–2000) at each station located in open terrain (top) rain-shadow terrain (middle) and windward terrain (bottom), simulated with the reference model version (left) and the new model version (right).*

## 3.3 Discussion

The mean annual precipitation maps show that the new model version produces more precipitation than the reference version in southern Iceland, on southern windward slopes and less precipitation on northerly lee slopes. Precipitation is usually lower in the northern half of the domain, especially over Snæfellsnes peninsula, the West-fjords (NW Iceland), Tröllaskagi massif (North) and the NE, which could be related to the reduction of the water vapor flux downwind, in the new model version. The same conclusion holds for the minimum and maximum annual precipitation and for the mean monthly precipitation except from May to July where precipitation is mostly lower everywhere in the new data set (Appendix-VII). Finally, the results indicate that the range of variation between minimum and maximum precipitation over the 15-year period can be quite substantial and that it is more pronounced over complex terrain with the new data set which also means a larger inter-annual variability.

Annual precipitation is better simulated with the new model version than the reference model in open and windward terrain, including the extreme values. In rain-shadow terrain, the results are relatively similar between the two data sets but the reference model has a slight advantage, indicating that the lee drying is more realistic in the reference model than the new model version. Similar results are observed for monthly precipitation and 3-day precipitation, a better simulation is achieved with the new model version except in rain-shadow terrain. Monthly precipitation simulated with the new model version appears to be more biased than for the reference model in DJF and MAM than in JJA and SON (Appendix I) which could also be related to wind-loss correction problems when snow and strong wind prevail. Note also that the quality of the simulations becomes poorer for both reference and new model versions with decreasing integration time, as expected.

The statistical characteristics of strictly positive daily precipitation calculated for each year are better reproduced overall with the new data set than the reference model, for the 25%, 50%, 75%, 90% and 95% quantiles, and very similar in quality for the mean, with a slight advantage for the reference model. Results differ slightly, however, depending on the type of topographical environment and the simulations made with the reference model provide better mean, 90% and 95% quantiles for stations located in rain-shadow. The number of wet days above 0.1 mm/day is slightly overestimated in the new data set compared with the reference model, at stations located in open and windward terrain. Similar results are observed when the quantiles are calculated over the entire 15-year period (Appendix V).

Results on the glaciers are usually superior with the reference model, but not systematically (Appendix II to IV). The new model version overestimates winter precipitation on glaciers, in average, while simulated precipitation at raingauge stations has improved at all temporal scales. These results could indicate that either the mass-balance data or the wind-corrected precipitation at raingauge stations are biased. The wind-loss precipitation correction may be overestimated during snowfall under strong wind. On the other hand, mass-balance data are also uncertain for a number of reasons such as the uncertainty about snow density, because of the difficulty to clearly identify the lower snow layer from previous year and therefore the snowdepth and because some of the snow that falls is not accounted for. However, these errors are not expected to lead to a systematic over- or under- estimation of the mass balance. In fact, the mass-balance data are regarded as a powerful dataset that should help to constrain the precipitation estimates. The

results may indicate that the statistical test used to select the best overall model set-up may have somehow over-represented the raingauge data and under-represented the mass-balance data.

# 4 Conclusion

The methodology employed at IMO to simulate precipitation fields with the Smith and Barstad (2004) Linear Model of orographic precipitation was revised. The new model set-up was verified over a 15-year period (1987–2001) and compared with previous simulations described in Jóhannesson et al. (2007). The results indicate that the new model version, which includes additional parameterization, has led to some improvements in the overall quality of the precipitation estimates. This methodology should be used to create a new precipitation climatology from 1958 to 2010. However, the need for parameterizing the humidity factor and the time scales for cloud water conversion, $\tau_c$, and hydrometeor fallout, $\tau_f$, still requires an optimization procedure and it will be interesting to first test whether this optimum parameterization holds for the entire period 1958–2010.

Using the model without a-priori fixing the hydrometeor formation and fallout times and the moist Brunt-Väisälä frequency should provide an advantage in the model applications, both in operational use, such as the dynamical downscaling of radar-based quantitative precipitation estimates (QPE), as suggested in Crochet (2009), and climate research, such as the dynamical downscaling of future climate scenarios for instance. Such a climatic application was recently considered in Carlotti and Barstad (2010) where the Linear Model was used to downscale 12 GCM simulations in western Norway for which the moist Brunt-Väisälä frequency was directly available but the cloud conversion and fallout times were arbitrarily set.

The model simulations are quite sensitive to the input atmospheric conditions which have to be domain-averaged and whose estimation will depend on the selection of the averaging domain and their spatial variability. The uncertainty resulting from this alone could be of the same order of magnitude or larger than the expected gain of accuracy resulting from using time varying $N_m$, $\tau_c$ and $\tau_f$ rather than constant optimized values.

In practise, although one specific model set-up was selected amongs an ensemble of possibilities, the results have shown that a unique best solution cannot be obtained for all features of the precipitation fields, which can be due to various reasons ranging from ground truth quality issues to input meteorological uncertainties and model physics. A new multi-objective view of the model calibration problem has emerged in the last decade or so (see for instance Gupta et al, 1998). The usefulness of such an approach will be further investigated in a future research.

# 5 Acknowledgements

This study was carried out within the framework of the Nordic Climate and Energy System research project (CES) and the corresponding Icelandic national project (LOKS), whose main objectives are to make a comprehensive assessment of the impact of climate change on renewable energy resources in the Nordic countries. The CES project is funded by Nordic Energy Research and the Nordic energy sector while the LOKS project is funded by Landsvirkjun (the National Power Company of Iceland), the Icelandic Road Administration and the National Energy Au-

thority. The author is grateful to Helgi Björnsson and Finnur Pálsson from the Science Institute of the University of Iceland for providing glaciological data from Vatnajökull and Langjökull.

# 6 References


Atladóttir, A., Crochet, P., S. Jónsson, S. & Hróðmarsson, H. B. (2011). *Mat á flóða-greiningu með rennslisröðum reiknuðum með vatnafræðilíkaninu WaSiM. Frumniðurstöður fyrir vatnasvið á sunnanverðum Vestfjörðum.* Reykjavík: Icelandic Meteorol. Office, Report VÍ-2011-008.

Barstad., I. & Smith, R. B. (2005). Evaluation of an orographic precipitation model. *J. Hydrometeor*, 6, 85–99.

Carlotti, G. N. & Barstad, I. (2010). An assessment of future extreme precipitation in western Norway using a linear model. *Hydrol. earth. Syst. Sci*., 14, 2329–2341.

Crochet, P., (2009): Enhancing radar estimates of precipitation over complex terrain using information derived from an orographic precipitation model. *J. Hydrol*., 377, 417–433.

Crochet, P., Jóhannesson, T., Jónsson, T., Sigurðsson, O., Björnsson, H., Pálsson, F., Barstad, I. (2007). Estimating the spatial distribution of precipitation in Iceland using a linear model of orographic precipitation. *J. Hydrometeor*., 8, 1285–1306.

Durran, D. R. & Klemp, J. B. (1982). On the effects of moisture on the Brunt-Väisälä frequency. *J. Atmos. Sci*., 39, 2152–2158.

Gupta, H. V., Sorooshian, S. & Yapo, P. O. (1998). Toward improved calibration of hydrologic models: multiple and noncommensurable measures of information. *Water Resour. Res*., 34(4), 751–763.

Jarosch, A. H., Anslow, F. S. & Clarke , G. K. C. (2010). High-resolution precipitation and temperature downscaling for glacier models. *Clim. Dyn*., DOI 10.1007/s00382-010-0949-1.

Jóhannesson T., Aðalgeirsdóttir, G., Björnsson, H., Crochet, P., Elíasson, E. B., Guðmundsson, S., Jónsdóttir, J. F., Ólafsson, H., Pálsson, F., Rögnvaldsson, Ó., Sigurðsson, O., Snorrason, Á., Blöndal Sveinsson, O. G. & Thorsteinsson, T. (2007). *Effect of climate change on hydrology and hydro-resources in Iceland.* Reykjavík: National Energy Authority, Report OS-2007/011.

Kunz, M., & Kottmeier, C. (2006). Orographic enhancement of precipitation over low mountain ranges. Part I: Model formulation and idealized simulations. *J. Appl. Meteor. Climatol*., 45, 1025–1040.

Sinclair, M. R., (1994): A diagnostic model for estimating orographic precipitation. *J. Appl. Meteor*., 33, 1163–1175.

Smith, R.B., & Barstad, I. (2004). A linear theory of orographic precipitation. *J. Atmos. Sci.*, 61, 1377–1391.

Smith, R. B., Barstad, I. & Bonneau, L. (2005). Orographic precipitation and Oregon's climate transition. *J. Atmos. Sci*., 62, 177–191.

Smith, R. B. & Evans, J.P. (2007). Orographic precipitation and water vapor fractionation over the southern Andes. *J. Hydrometeor*., 8, 3–19.

Schuler, T. V., Crochet, P., Hock, R., Jackson, M., Barstad, I. & Jóhannesson, T. (2008). Distribution of snow accumulation on Svartisen ice cap (Norway) assessed by a model of orographic precipitation. *Hydrological Processes*, 22, 3998–4008.

Uppala, S. M. (2005). The ERA-40 re-analysis. *Q.J. R. Meteorol. Soc.*, 131, 2961–3012.